Multifunctional Barium Titanate Coated Carbon Fibers

*Christopher Bowland, Zhi Zhou, and Henry A. Sodano**

Multifunctional materials have received significant research interest due to the potential for performance enhancements over traditional materials through the integration of responsive properties. Composite materials are ideally suited for use as multifunctional materials due to their use of two or more phases and the ease at which their properties can be anisotropically tailored. Here, a methodology for the integration of ferroelectricity into a fiber reinforced polymer composite is presented by synthesizing a barium titanate nanowire film on the surface of carbon fibers using a novel two-step hydrothermal process. A refined piezoelectric force microscopy method is used to quantify the piezoelectric properties of the core–shell fiber resulting in an average d_{33} of 31.6 ± 14.5 pm V^{-1} and an average d_{31} of −5.4 ± 3.2 pm V^{-1}. The multifunctionality of this piezoelectric coated fiber is demonstrated through excitation of a cantilevered fiber with a 0.5 *g* sinusoidal base acceleration at the fiber's fundamental resonant frequency, producing a root-mean-square voltage of 16.4 mV. This result demonstrates the ferroelectric properties of the multifunctional structural fiber and its application for sensing and energy harvesting.

1. Introduction

Multifunctional composites are designed to meet multiple performance objectives by modifying or improving the strength of the composite while contributing additional functionality, such as structural health monitoring,[1] actuation,[2–6] sensing,[7–9] power generation and storage,[10,11] ballistic protection,[12] and vibration damping.[13,14] Each of these applications can be achieved using piezoelectric materials due to their coupling between energy in the mechanical and electrical domains. Research into the creation of multifunctional materials with embedded piezoelectricity dates back to 1993 when solid lead zirconate titanate (PZT) fibers were embedded into a fiberglass reinforced plastic.[3,4] This early work demonstrated the clear potential for embedded piezoelectric materials to create functional structures. However, early studies into the development of functional piezoelectric composites lead to significant reduction in material strength due to the brittle nature of the piezoceramic fibers and their considerably larger diameter than the reinforcing materials.

More recently, Lin et al. developed an active structural fiber composed of a silicon carbide fiber core surrounded by a barium titanate ($BaTiO_3$) shell to serve as functional reinforcement for composites. The fiber minimized the complexity of the system by acting as the internal electrode, and the electromechanical coupling was characterized along with the capacitive energy storage properties.[15–17] The fiber demonstrated excellent performance, but its 300 µm diameter still led to defects once embedded into a composite material. There exists a critical need to create multifunctional components which have the same dimension as high-performance reinforcing materials, such as carbon fiber. However, the primary challenge lies in the lack of methods to conformably coat a 5 µm carbon fiber with a crack-free piezoceramic.

Recently, Zhou et al. developed a method for the hydrothermal growth of vertically aligned $BaTiO_3$ nanowires on fluorine-doped tin oxide glass with a reported d_{33} value of 43 ± 2 pm V^{-1}.[18] The relatively low-temperature, aqueous solution-based characteristics of the hydrothermal reaction enable piezoceramic growth on a wide variety of materials of various dimensions and shapes. This provides a method to uniformly deposit a piezoceramic material on the surface of thousands of fibers simultaneously. The homogeneous dispersion of ions in the solution allow for nucleation and growth on every fiber in the solution with complete surface coverage. Additionally, hydrothermally synthesized $BaTiO_3$ nanowire arrays have demonstrated performance improvements in power harvesting applications as compared to popularly researched ZnO nanowire arrays. Recently, Koka et al. reported that an energy harvester composed of $BaTiO_3$ nanowires showed a 16-fold improvement in power density over an energy harvester composed of zinc oxide (ZnO) nanowires, and a 20-fold performance increase in sensitivity was realized from a $BaTiO_3$ nanowire-based sensor as compared to a ZnO nanowire-based device.[19,20] By combining these performance enhancements realized from $BaTiO_3$ nanowires with a strong reinforcing fiber, such as carbon fiber, there is the opportunity to create a new structural multifunctional fiber that meets the small dimensional requirements of high-performance, fiber-reinforced polymer composites while adding functionality to the composite.

In this paper, a two-step processing procedure is used to grow a $BaTiO_3$ nanowire film on carbon fiber. This processing

C. Bowland, Z. Zhou, Dr. H. A. Sodano
Department of Materials Science and Engineering
University of Florida
Gainesville, FL 32611, USA
E-mail: hsodano@ufl.edu
Dr. H. A. Sodano
Department of Mechanical and Aerospace Engineering
University of Florida
Gainesville, FL 32611, USA

DOI: 10.1002/adfm.201401417

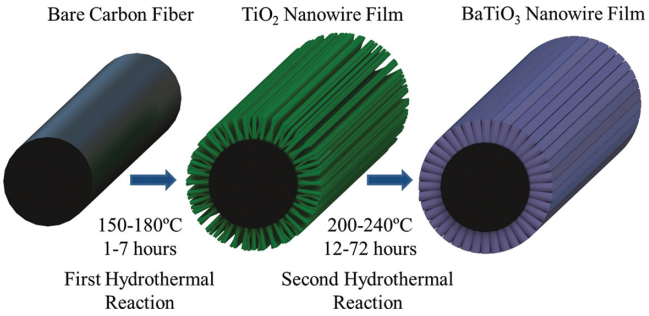

Figure 1. Schematic illustration of the two-step hydrothermal process to synthesize TiO_2 and $BaTiO_3$ nanowire films on carbon fiber.

technique is performed at relatively low temperatures in order to maintain the structural integrity of the carbon fiber thus preserving its viability as a structural multifunctional fiber. The electromechanical coupling coefficient of the $BaTiO_3$ is measured using a refined piezoelectric force microscopy (PFM) testing method. This research demonstrates the ability to grow $BaTiO_3$ on carbon fiber while maintaining its strength and illustrates an unconventional method for characterizing a conformal film of a piezoceramic material on a non-planar substrate thus enabling potential applications in structural health monitoring, power harvesting, sensing, and microelectromechanical systems.

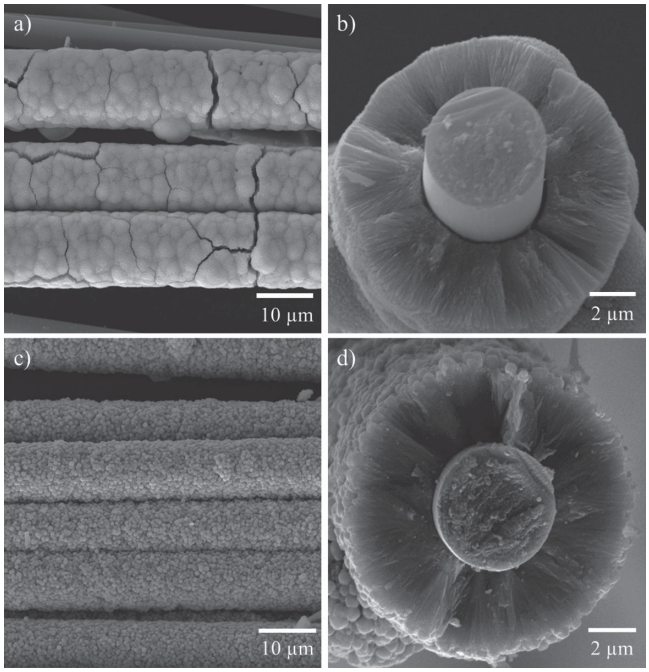

Figure 2. a) TiO_2 coated carbon fiber. b) Cross section of the TiO_2 nanowire film showing the densely packed nanowire growth normal to the carbon fiber surface. c) $BaTiO_3$ coated carbon fiber. d) Cross section of the $BaTiO_3$ showing a dense nanowire film surrounding the carbon fiber core.

2. Results and Discussion

A $BaTiO_3$ nanowire film was synthesized on carbon fiber through a two-step hydrothermal reaction as illustrated in the schematic in **Figure 1**. The initial step to the conformal growth of $BaTiO_3$ on the surface of a carbon fiber is the synthesis of an array of vertically aligned TiO_2 nanowires that act as a precursor template. Prior to nanowire growth, a titanium sol–gel is applied to the fiber surface through dip coating and thermal annealing to crystalize the film, which creates a seed layer of TiO_2 nanoparticles on the fiber surface that assist in nanowire nucleation. This step is not critical to the conformal growth of the film however leads to more dense nucleation and thus improved alignment and uniformity of the film. The seeded fibers are then placed in an acid digestion bomb that is heated which leads to the crystallization of vertically aligned arrays of TiO_2 nanowires. **Figure 2**a,b illustrates the dense array of aligned rutile TiO_2 nanowires that grow radially outward from the carbon fiber surface. It should be noted that there are cracks in the TiO_2 nanowires array that are filled during the conversion process to barium titanate. The second hydrothermal reaction converts the TiO_2 nanowires to $BaTiO_3$ and alters the nanowire morphology to a conformal nanowire film. The conversion step involves a dissolution/precipitation process in which the surface of the TiO_2 nanowire is hydrolyzed into $Ti(OH)_6^{2-}$ which reacts with the Ba^{2+} ions in the solution to precipitate a $BaTiO_3$ layer. Subsequent conversion to $BaTiO_3$ is achieved through a classical diffusion mechanism through the TiO_2 nanowires driven by the high pressure conditions and Ba^{2+} concentration gradient within the closed hydrothermal reaction container.[21–24] The diffusion of the larger Ba^{2+} ion increases the volume of the original TiO_2 crystal lattice due to the size differences in ionic radii (Ba^{2+} 0.149 nm, Ti^{4+} 0.060 nm, and O^{2-} 0.126 nm) thus causing the $BaTiO_3$ nanowires to expand into the voids between the TiO_2 nanowires. As shown in Figure 2c,d, nanowire expansion causes the discontinuities in the TiO_2 nanowire coating to fill in and create a continuous, crack-free $BaTiO_3$ nanowire film. Despite this expansion during conversion, the preferred orientation of the nanowires is preserved. Therefore, the TiO_2 nanowires act as a template for creating a textured nanowire film of $BaTiO_3$.[25]

2.1. Crystal Structure and Mechanical Testing

To confirm the conversion from TiO_2 to $BaTiO_3$, the resultant samples from the first and second hydrothermal reactions were tested by X-ray diffraction (XRD). The XRD patterns of the first hydrothermal reaction samples (**Figure 3**a) indicate the growth of rutile TiO_2 through the strong peaks at 27°, 36°, and 55°, which match the Joint Committee on Powder Diffraction Standards (JCPDS) Card No. 65–0190.[26] Due to the amorphous nature of the carbon fiber, a low-intensity, broad peak appears below 30°. The XRD pattern of the sample after conversion (Figure 3a) shows distinguishable diffraction peaks at 32°, 39°, and 45° which are representative of $BaTiO_3$ according to JCPDS Card No. 05–0626. Single fiber tensile testing was performed after each processing step to investigate any alterations in the ultimate tensile strength of the fiber. As illustrated in Figure 3b, the fiber experienced no significant decrease in tensile strength after the pre-growth sol–gel process or after TiO_2 nanowire growth, and the $BaTiO_3$ conversion process retained 74% of

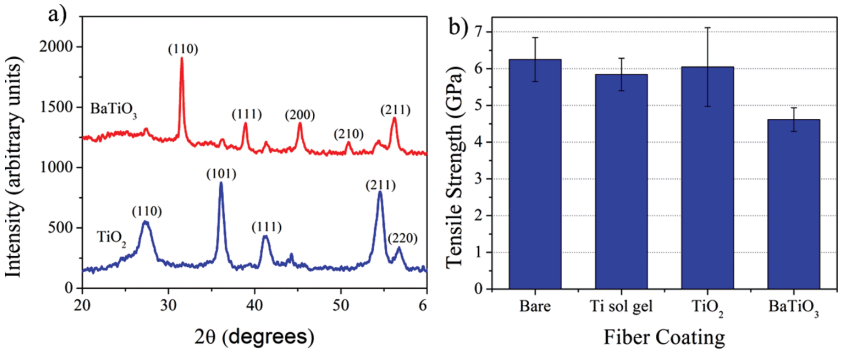

Figure 3. a) The TiO_2 to $BaTiO_3$ conversion is confirmed by the characteristics peaks seen in the XRD patterns and b) tensile tests reveal no change in the tensile strength during the TiO_2 growth and the $BaTiO_3$ coated fibers maintain most of their strength after conversion.

the original tensile strength. The average tensile strength of the bare carbon fiber was 6.25 GPa and maintained an average tensile strength of 4.62 GPa after $BaTiO_3$ conversion thus allowing it to remain useful as a structural fiber. Therefore, the multifunctional fibers created here are the strongest fibers to date utilizing the piezoelectric and ferroelectric property of $BaTiO_3$ to create additional functionality.

2.2. Electromechanical Testing

Conventional techniques for measuring the piezoelectric coefficients of bulk piezoelectric materials are the Berlincourt method and laser interferometry. These techniques work best when probing flat surfaces that allow for better surface contact and better reflection from the surface for the Berlincourt method and laser interferometry, respectively.[27,28] Due to the nano-scale dimensions and curvature of the $BaTiO_3$ nanowire film in this research, the Berlincourt method and laser interferometry are not viable techniques for accurately measuring the piezoelectric coefficients. So the development of new electromechanical characterization methods is required for continuing progress in the field. To solve this problem, an atomic force microscope (AFM) in piezoelectric force microscopy (PFM) mode can be used in the characterization of nano-scale piezoelectric materials through detection of the sample surface displacement induced by an applied electric field. In order to accurately measure the piezoelectric behavior of the $BaTiO_3$ nanowire film, a refined AFM testing method has been developed in previous research by using the AFM as a displacement sensor and applying a filtering and averaging scheme over numerous cyclic measurements.[18]

An additional advantage of the refined PFM method is that it allows for the investigation of both the d_{33} and d_{31} piezoelectric coefficients. By applying an external voltage to the nanowire film, the mechanical strain response of the $BaTiO_3$ can be measured by the AFM tip due to the converse piezoelectric effect defined by

$$\varepsilon_j = d_{ij} * E_i \quad (1)$$

where ε_j is the strain, d_{ij} is the piezoelectric coupling coefficient, and E_i is the applied electric field. By defining the 3-direction as the direction normal to the axial direction of fiber, the d_{33} piezoelectric coefficient measures the strain in the 3-direction induced from an electric potential in the 3-direction as shown in **Figure 4**a. Prior to electromechanical testing, the fibers were poled using a corona discharge technique as described by Waller et al. in order to align the electric dipoles along the 3-direction.[29] Then an AFM topography scan in non-contact mode with a low scan speed (0.3 μm s^{-1}) was performed (Figure 4c) to locate the absolute top facet of the nanowire film. Upon locating this position, the AFM was switched to contact mode and a 1 Hz triangle wave was supplied by a function generator (Agilent, 33210A) to the carbon fiber core and grounded through the conductive AFM tip. In order to reduce any potential electrostatic forces between the AFM tip and the $BaTiO_3$, a force of 1500 nN was held between the tip and sample during testing. Repetition of the same process on a silicon wafer, which is not piezoelectric, showed no displacement response to the applied field, thus confirming that the AFM cantilever was not being deflected by the applied electric field. Therefore, the displacement shown for the $BaTiO_3$ samples was from the converse piezoelectric effect. For d_{31} measurements, the electric field is still applied in the 3-direction, but the displacement is measured in the 1-direction which is in the axis of the fiber as shown in Figure 4b. The electric field is directly applied to the $BaTiO_3$ through a gold coating sputtered around the entire circumference of the nanowire film, while a grounded conductive AFM is located on the top facet of carbon fiber to ground the core carbon fiber electrode. To reduce the noise and error in the d_{33} and d_{31} values, the data was processed through a band pass filter and the average displacement responses of at least 50 voltage cycles were reported. By plotting the displacement as a function of applied electric field as shown in Figure 4d, the slope of the curves provided the effective d_{33} and d_{31} values of the $BaTiO_3$. This testing resulted in an average effective d_{33} of 31.6 ± 14.5 pm V^{-1} with a maximum achievable value of 61.8 pm V^{-1} and an average effective d_{31} of −5.4 ± 3.2 pm V^{-1} with a maximum achievable value of −12.9 pm V^{-1}. These values are less than the reported values for bulk $BaTiO_3$ of 85.6 pm V^{-1} and −34.5 pm V^{-1} for d_{33} and d_{31}, respectively.[30] This reduction is attributed to substrate clamping effects, which have been shown to reduce the piezoelectric response by restricting domain wall motion close to the substrate-piezoceramic material interface and is pronounced in thin films such as those synthesized here.[31] The piezoelectric strain coefficients measured here closely match the strain coefficients of 40–70 pm V^{-1} previously measured in clamped $BaTiO_3$ films.[32] To investigate the ferroelectric property of the $BaTiO_3$ film, phase change and butterfly loop plots were gathered from the AFM by applying a bipolar electric field (Figure 4e,f). A slight asymmetry is observed in these plots, which may be attributed to internal stresses. The expansion of the TiO_2 nanowires during the conversion process to $BaTiO_3$ may induce internal stresses. These stresses cause uneven clamping within the film producing an asymmetric ferroelectric response.[33,34] Despite

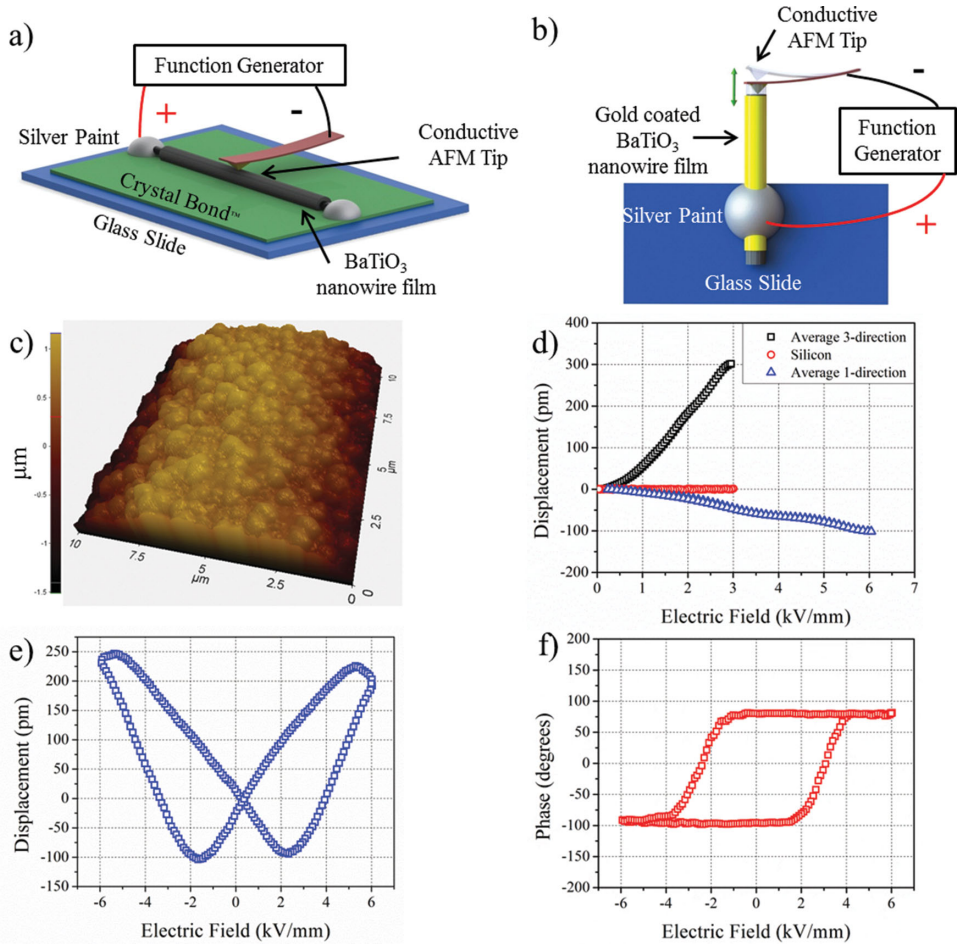

Figure 4. Schematic representations of the fiber configurations for a) d_{33} and b) d_{31} AFM testing. c) Topography scan of the $BaTiO_3$ in the d_{33} test setup d) The resulting displacement measurements during the application of a unipolar electric field. Ferroelectric property was observed from bipolar excitation in the d_{33} setup in the e) butterfly loop and f) phase change plot showing a 180° phase shift.

the slight asymmetry, this demonstrates that the $BaTiO_3$ film is ferroelectric due to the electric field's ability to reversibly change the direction of spontaneous polarization in the crystal.

2.3. Vibration Excitation

The piezoelectric properties of the fiber were further validated through a cantilevered sample as shown in **Figure 5**a. The cantilevered fiber was attached to a permanent magnet shaker and white noise excitation was used to a obtain power spectral density plot and a phase change plot of the fiber's output voltage as seen in Figure 5b. These plots indicate a resonant frequency at 52 Hz, which is revealed through a peak in the voltage spectral power density plot and a 180 degree phase change at 52 Hz. Consequently, the sample was excited with a sinusoidal wave at the fundamental resonant frequency (52 Hz) to generate an enhanced output voltage response while excitation acceleration measured by an instrumentation-grade shear accelerometer (PCB352C22) and voltage response curves were simultaneously recorded in Figure 5d,e. This resulted in a root-mean-square voltage response of 16.4 mV from a root-mean-square acceleration input of 0.5 g. As further evidence for the power harvesting and sensing potential of this fiber, the excitation was terminated during the test and the voltage output from the piezoelectric response of the cantilever slowly decreased as the oscillation of the fiber dampened to return to a steady-state position as shown in Figure 5c. These results demonstrate the potential application of this structural multifunctional fiber in power harvesting applications that require relatively low frequency ranges. For example, typical ambient vibration frequencies lie in the sub-kHz range, so the development of a piezoelectric device that can operate at these low frequency ranges is highly desirable.[35] Additionally, the cantilever design allows for the tuning of the resonant frequency by adjusting the length of the cantilever thus enabling the device to be tailored to various low-frequency applications. Therefore, this multifunctional carbon fiber opens up applications for piezoelectrics that were previously unattainable due to frequency limitations caused by the stiffness of the piezoelectric material in its bulk form.

3. Conclusion

A $BaTiO_3$ nanowire film was successfully grown on carbon fiber by a two-step hydrothermal process that enabled the fiber to

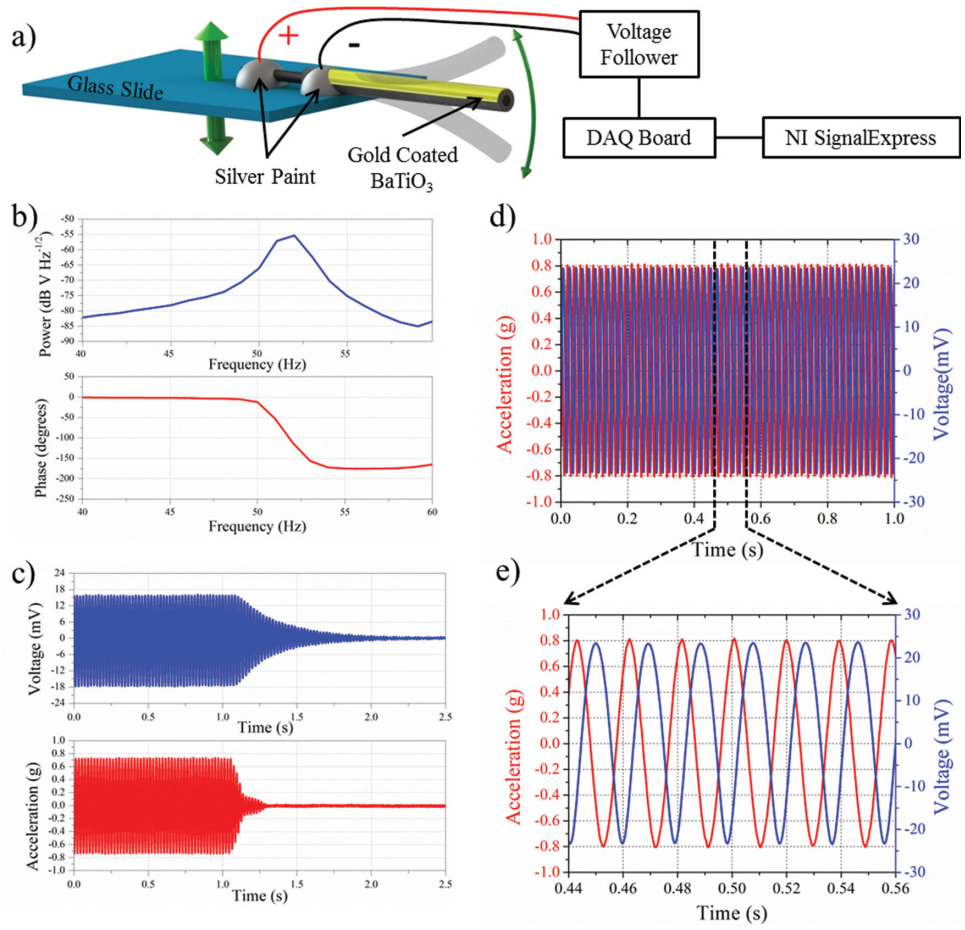

Figure 5. a) The schematic representation of the cantilevered fiber for vibration excitation. b) Voltage spectral power density and phase change plots indicate a resonant frequency at 52 Hz. c) Termination of the input acceleration results in a dampening of the voltage response from the cantilever. d) 52 Hz excitation produces a root-mean-square voltage response of 16.4 mV under 0.5 *g* root-mean-square base acceleration. e) Expanded view of the sinusoidal excitation and response shows a 90° phase lag between piezoelectric electric output and input acceleration.

maintain 74% of its original tensile strength. A refined piezoelectric force microscopy testing method was utilized to characterize its electromechanical properties resulting in a maximum d_{33} of 61.8 pm V^{-1} with an average of 31.6 ± 14.5 pm V^{-1} and a maximum d_{31} of –12.9 pm V^{-1} with an average of –5.4 ± 3.2 pm V^{-1}. Exciting a cantilevered fiber on a permanent magnet shaker proved that the fiber could operate at relatively low frequencies thus enabling potential real-world vibrational energy harvesting applications. This research demonstrates the development of a structural multifunctional fiber that meets the dimensional and strength specifications of reinforcing components in today's high-performance, fiber-reinforced polymer composites while providing additional power harvesting and sensing capabilities.

4. Experimental Section

Hydrothermal Growth: The $BaTiO_3$ nanowire film was formed through a two-step hydrothermal reaction. The first step utilized a solution containing a 1:2 volume ratio of titanium tetrachloride (Alfa Aesar, 99.0%) and titanium isopropoxide (Alfa Aesar, VERTEC TIPT, 97+%) in a 1:1 volume ratio of concentrated hydrochloric acid (Fisher, 35%) and DI water. Prior to TiO_2 growth, the carbon fibers (Hexcel IM8) were seeded using a titanium sol–gel containing concentrated hydrochloric acid, isopropanol, and titanium isopropoxide. The fibers were dipped in the titanium sol–gel and annealed at 120 °C for 1 h. The solution and carbon fiber tow were placed in a Teflon vessel and encased in a steel enclosure. The solution was heated to between 150 °C and 180 °C for 1 hour to 7 hours to produce a TiO_2 nanowire array. This method is described in more detail by Liu et al.[36] This TiO_2 nanowire array was then converted to $BaTiO_3$ during a second hydrothermal reaction using an aqueous solution containing a barium source as described by Zhou et al.[25] This step was carried out at temperatures between 200 °C and 240 °C for 12 h to 72 h.

Characterization: X-ray diffraction (XRD) was performed on the fibers using an X-ray diffractometer (CPS120, Inel) equipped with a curved position-sensitive detector and a CuKα X-ray tube source. The morphologies of the samples were examined using a scanning electron microscope (SEM, TESCAN VEGA3 LM). Tensile testing was performed according to ASTM Standard C 1557–03 using a table top automated electro-mechanical testing system (Instron 5567). To determine the effect of processing on the mechanical strength of the fibers, testing was performed on as-received, titanium sol–gel coated, TiO_2 coated, and $BaTiO_3$ coated carbon fibers. Electromechanical testing was performed in an AFM using an electrically conductive dynamic contact electrostatic force microscopy tip (Park AFM XE-70, DC-EFM). A lock-in amplifier (Stanford Instruments SR830) was used in conjunction with

the AFM. An applied AC signal frequency of 17 kHz was chosen to avoid unnecessary topographic crosstalk near the cantilever resonance. A 1 Hz sinusoidal wave was supplied using a function generator (Agilent 33210A). Individual $BaTiO_3$ coated fibers were mounted with CrystalBond on glass slides which were subsequently attached to conductive AFM pucks. For d_{33} measurements, the fibers were adhered to the glass slide with the axial direction parallel to the surface of the glass slide. This mounting orientation exposed the surface normal to the axial direction thus probing the displacement response in the same direction as the electric field was applied. Removing the $BaTiO_3$ coating from the fiber core using a razor blade allowed the carbon fiber to be contacted with silver paint and electrically connected to the AFM puck. This served as the bottom electrode during AFM testing. The DC-EFM tip acted as the top electrode. For d_{31} measurements, the fiber was in the same orientation as the d_{33} testing, but the fiber was extended beyond the edge of the glass in order to have an unconstrained section that was able to expand and contract as an electric field was applied. In this case, gold was sputtered using a PELCO SC-7 Auto Sputter Coater on the entire circumference of the fiber and contacted by silver paint. The AFM tip contacted the carbon fiber core at the unconstrained end of the fiber to act as the second electrode. These setups are illustrated in Figure 4a,b.

Vibration Testing: The sinusoidal wave excitation and voltage response setup consisted of a miniature permanent magnet shaker (Labworks, Inc. ET-132). The sample was placed inside a Faraday cage on top of the shaker and connected to a high impedance (1TΩ) voltage follower, which was constructed using a Linear Technologies Op Amp (LTC6240CS8CMOS). Next to the sample, a commercial shear accelerometer (PCB 352C22) was attached to measure the input base acceleration. The top of the fiber was sputtered with gold and contacted with silver paint in order to create the top electrode while the carbon fiber core was also contacted with silver paint to act as the bottom electrode. The signals were generated and acquired through a DAQ board (NI USB 4431) in conjunction with NI SignalExpress software.

Acknowledgements

The authors thank the Air Force Office of Scientific Research and Dr. B. L. Lee for support for this research.

Received: May 1, 2014
Revised: June 24, 2014
Published online: August 13, 2014

[1] C. Li, T. Chou, *Compos. Sci. Technol.* **2008**, *68*, 3373–3379.
[2] I. Kang, Y. Y. Heung, J. H. Kim, J. W. Lee, R. Gollapudi, S. Subramaniam, S. Narasimhadevara, D. Hurd, G. R. Kirikera, V. Shanov, *Compos. Part B: Eng.* **2006**, *37*, 382–394.
[3] A. A. Bent, N. W. Hagood, J. P. Rodgers, *J. Intell. Mater. Syst. Struct.* **1995**, *6*, 338–349.
[4] N. Hagood, A. Bent, *AIAA Paper.* **1993**, (93–1717), 3625–3638.
[5] G. A. Sotiriou, C. O. Blattmann, S. E. Pratsinis, *Adv. Funct. Mater.* **2013**, *23*, 34–41.
[6] J. M. Haberl, A. Sánchez-Ferrer, A. M. Mihut, H. Dietsch, A. M. Hirt, R. Mezzenga, *Adv. Funct. Mater.* **2014**, *24*, 3179–3186.
[7] J. Tressler, S. Alkoy, A. Dogan, R. Newnham, *Compos. Part A: Appl. Sci. Manufact.* **1999**, *30*, 477–482.
[8] H. A. Sodano, G. Park, D. J. Inman, *Mech. Syst. Signal Proc.* **2004**, *18*, 683–697.
[9] S. Gao, R. Zhuang, J. Zhang, J. Liu, E. Mäder, *Adv. Funct. Mater.* **2010**, *20*, 1885–1893.
[10] Y. Lin, H. A. Sodano, *Compos. Sci. Technol.* **2008**, *68*, 1911–1918.
[11] H. A. Sodano, D. J. Inman, G. Park, *Shock Vib. Dig.* **2004**, *36*, 197–206.
[12] K. S. Vecchio, *JOM,* **2005**, *57*, 25–31.
[13] S. Raja, G. Prathap, P. Sinha, *Smart Mater. Struct.* **2002**, *11*, 63.
[14] V. P. Veedu, A. Cao, X. Li, K. Ma, C. Soldano, S. Kar, P. M. Ajayan, M. N. Ghasemi-Nejhad, *Nat. Mater.* **2006**, *5*, 457–462.
[15] Y. Lin, H. A. Sodano, *Compos. Sci. Technol.* **2009**, *69*, 1825–1830.
[16] Y. Lin, H. A. Sodano, *J. Appl. Phys.* **2009**, *106*, 114108–114108–5.
[17] Y. Lin, H. A. Sodano, *Adv. Funct. Mater.* **2009**, *19*, 592–598.
[18] Z. Zhou, H. Tang, H. A. Sodano, *ACS Appl. Mater. Interfaces* **2013**, *5*, 11894–11899.
[19] A. Koka, Z. Zhou, H. Sodano, *Energy Environ. Sci.* **2014**, *7*, 288–296.
[20] A. Koka, H. A. Sodano, *Nat. Commun.* **2013**, *4*.
[21] W. Hertl, *J. Am. Ceram. Soc.* **1988**, *71*, 879–883.
[22] R. Bacsa, P. Ravindranathan, J. Dougherty, *J. Mater. Res.* **1992**, *7*, 423–428.
[23] M. Yoshimura, S. Yoo, M. Hayashi, N. Ishizawa, *Jpn. J. Appl. Phys.* **1989**, *28*, L2007.
[24] E. Ciftci, M. Rahaman, M. Shumsky, *J. Mater. Sci.* **2001**, *36*, 4875–4882.
[25] Z. Zhou, Y. Lin, H. Tang, H. A. Sodano, *Nanotechnology* **2013**, *24*, 095602.
[26] K. Thamaphat, P. Limsuwan, B. Ngotawornchai, *Kasetsart J. Nat. Sci.* **2008**, *42*, 357–361.
[27] Q. Zhang, W. Pan, L. E. Cross, *J. Appl. Phys.* **1988**, *63*, 2492–2496.
[28] D. A. Berlincourt, F. Kulcsar, *J. Acoust. Soc. Am.* **1952**, *24*, 709.
[29] D. Waller, T. Iqbal, A. Safari, *J. Am. Ceram. Soc.* **1989**, *72*, 322–324.
[30] R. E. Newnham, *Properties of Materials: Anisotropy, Symmetry, Structure*, Oxford University Press, Oxford, New York **2005**.
[31] R. Torah, S. Beeby, N. White, *J. Phys. D* **2004**, *37*, 1074.
[32] V. Nagarajan, A. Roytburd, A. Stanishevsky, S. Prasertchoung, T. Zhao, L. Chen, J. Melngailis, O. Auciello, R. Ramesh, *Nat. Mater.* **2003**, *2*, 43–47.
[33] Z. Wang, Y. Yao, X. Wang, W. Yue, L. Chen, X. X. Zhang, *Sci. Rep.* **2013**, *3*, 3127.
[34] Y. Xu, Y. Feng, N. Zhang, *J. Am. Ceram. Soc.* **2011**, *94*, 3863–3866.
[35] N. Setter, *Electroceramic Based MEMS: Fabrication-Technology and Applications* Vol. *9*, Springer, New York **2005**.
[36] B. Liu, E. S. Aydil, *J. Am. Chem. Soc.* **2009**, *131*, 3985–3990.